JCTC Journal of Chemical Theory and Computation

Article

pubs.acs.org/JCTC

Implicit Solvent Models and Stabilizing Effects of Mutations and Ligands on the Unfolding of the Amyloid β-Peptide Central Helix

Alok Juneja, Mika Ito, and Lennart Nilsson*

Department of Biosciences and Nutrition, Center of Biosciences, Karolinska Institutet, SE-141 83 Huddinge, Sweden

Supporting Information

ABSTRACT: We have systematically evaluated the ability of molecular dynamics simulation with implicit solvation models (EEF1.1, SASA, ASPENR, SCPISM, RUSH, ACE2, GBORN, GBSW, GBMV II, FACTS) to characterize the unfolding of the amyloid beta (Aβ) peptide and the stabilizing effects of mutations and ligands. The 13−26 region of Aβ (Aβ_{13-26}) unfolds and leads to the formation of amyloid fibrils, the causative agent of Alzheimer's disease. Stabilization of Aβ_{13-26} decreases Aβ polymerization as well as the formation of intermediate structures, which may also be toxic. The unfolding behavior of wild-type Aβ_{13-26} with an increase in temperature led us to select GBORN, GBMV II, and SCPISM for further investigation considering their ability to reproduce the stabilizing effect on the Aβ_{13-26} helical conformation due to mutations (V18A/F19A/F20A and V18L/F19L/F20L) and ligands (Dec-DETA and Pep1b) designed to stabilize Aβ_{13-26}. Structural parameters (RMSD, helicity) of the peptide were used to assess the performance of the implicit solvent models with reference to previous explicit solvent simulations.

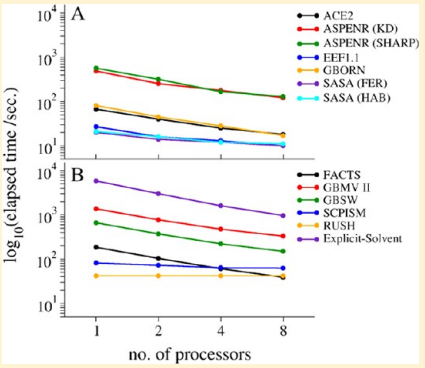

INTRODUCTION

Alzheimer's disease is the most common form of dementia in which a progressive deterioration of memory and other cognitive domains leads to death.[1] The amyloid beta peptide (Aβ) contains 36−43 amino acids and is most commonly known in association with Alzheimer's diesease.[1] Aβ is formed after sequential cleavage of an integral trans-membrane glycoprotein, the amyloid precursor protein, by successive action of β and γ secretases.[1]

A five residue segment in the middle of Aβ, $K_{16}LVFF_{20}$ (Aβ_{16-20}) constituting the hydrophobic stretch that promotes Aβ self-assembly, is capable of binding to full-length Aβ.[2−4] It has been reported in circular dichroism spectroscopy and electron microscopy studies that the α-helical content of residues 16−23 of Aβ_{12-28} is increased by substituting V18A/F19A/F20A, which leads to reduced fibril formation.[5] This finding has also been reported recently in simulation studies on helical forms of Aβ_{1-42} and its analogues.[6,7] To understand the detailed mechanism of the unfolding of the Aβ and its stabilization by V18A/F19A/F20A substitution,[5] simulation studies under aqueous solution conditions have been made on the 13−26 region of wild-type Aβ (Aβ_{13-26}, sequence: HHQKLVFFAEDVGS) as well as for the V18A/F19A/F20A and V18L/F19L/F20L helix-stabilizing mutants.[7] The Aβ_{13-26} is of interest since the $K_{16}LVFF_{20}$ motif is included in this region.

Molecular dynamics simulations are also used to investigate the influence of active drug candidates on the early phase of the aggregation of the Aβ hydrophobic core segment $K_{16}LVFF_{20}$ and to stabilize the hydrophobic core in its α-helical conformation.[8,9] Two different ligands, Dec-DETA and Pep1b (Figure 1),

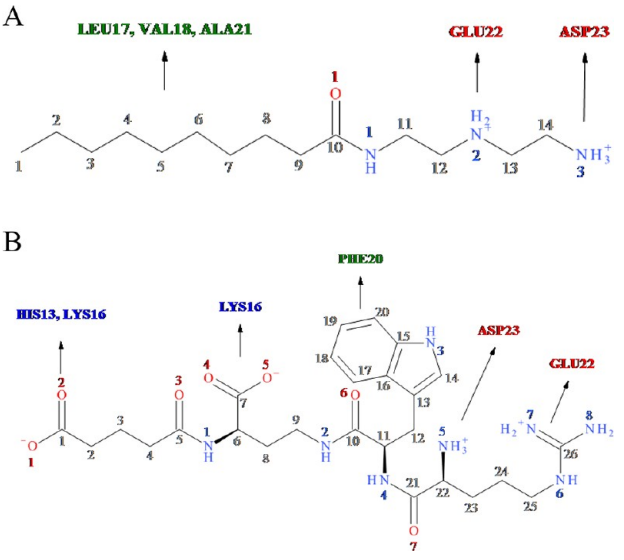

Figure 1. Chemical structures of ligands Dec-DETA (A) and Pep1b (B) are shown. The naming and numbering on ligands: carbon (gray), nitrogen (blue), and oxygen (red) atoms. The naming and numbering of Aβ_{13-26} residues is basic (blue), acidic (red), nonpolar (green), and uncharged-polar (black). Arrows indicate the interactions between mentioned residues of Aβ_{13-26} (head) and different groups of the ligands (tail).

designed to bind Aβ_{13-26},[10] were recently investigated using explicit solvent (ES) molecular dynamics simulations to

Received: October 30, 2012
Published: December 3, 2012

   dx.doi.org/10.1021/ct300941v | J. Chem. Theory Comput. 2013, 9, 834−846

understand the influence and detailed molecular mechanism of their stabilization of the helix in $A\beta_{13-26}$.[11]

The behavior of molecules in solution depends fundamentally on the balance of solute−solute versus solute−solvent and solvent−solvent interactions. The native structure of most biomolecules is governed by interactions with water,[12,13] and in order to adopt their native structure, which is a prerequisite to proper function,[14−18] biomolecules need to be under physiological conditions (i.e., specific temperature, pH, and ionic strength). Therefore, for realistic modeling of biomolecules, we must account for the effects of the solvent environment, which can be treated using an explicit solvent representation in which solvent molecules are modeled at the same level of detail as the biomolecules. A sufficiently large number of individual water molecules are placed around the solute, and their motion is simulated on an equal footing with the solute molecule of interest, thus providing a representative picture of how biomolecules behave in a biological cell. This is arguably the most realistic approach, but at the same time it suffers from considerable computational cost, a significant part of which comes from solvent−solvent interactions. Simulations based on this methodology are well established for the study of single biomolecules over nanosecond time scales but are often prohibitively slow, especially for the large biomolecular systems and long-time scale processes such as those involved in protein folding.[15,17,19,20]

Different procedures have been applied to reduce the CPU time required for MD simulations. One approach to accelerate simulations of biomolecules involves the application of a mean-field description of solute−solvent interactions rather than explicit solvent.[21] This implicit solvent methodology (IS)[21−26] reduces the number of atoms to be considered enormously since it represents the aqueous solvent environment using a high dielectric continuum medium with electrostatic properties that match water. Entropic (hydrophobic) and viscous effects can also be added. There have been a number of efforts in recent times to advance IS models to simulate biomolecules efficiently and to come close to the results of computationally more expensive conventional MD simulations with an ES model, as reviewed elsewhere on different biological systems.[27−34]

Implicit solvent represents a compromise between computational efficiency and the level of realism. An additional efficiency bonus of IS models is the absence of solvent viscosity, which means that motions are faster in the simulation than in reality. Hence, it allows exploration of the conformational space of a solute molecule in shorter simulation times, and several all-atom IS MD simulations of *ab initio* folding of small proteins are reported to gain insight into the protein folding mechanism[31,35−37] and to study large-scale motions in proteins and their complexes.[38,39]

In the present study, the focus is to evaluate the efficiency and efficacy of different IS models compared to recently performed ES simulation studies on the unfolding of wild-type $A\beta_{13-26}$ ($A\beta_{13-26}$-WT) and the stabilizing effect of mutations ($A\beta_{13-26}$-MA: V18A/F19A/F20A and $A\beta_{13-26}$-ML: V18L/F19L/F20L)[7] as well as of ligands (Dec-DETA and Pep1b) on the $A\beta_{13-26}$ helicity.[11] A specific aim is to identify a combination of IS model and simulation temperature that allows the detection of helix stability in MD simulations of defined length (100 ns in this case) using the same stability criteria as in the ES simulation.

THEORY AND METHODS

Implicit Solvent Models. Several reviews of implicit solvent methods have been published,[21,22,27−34,40] and here we only give a brief outline of the main concepts underpinning the most commonly used methods. There is always a trade-off between the accuracy and speed that has to be considered when using, or designing, an approximate method in molecular modeling applications. In the implicit solvent formalism, the total solvation energy is decomposed into polar and nonpolar contributions. Although the Poisson−Boltzmann equation (PB)[24,41−45] treats the continuum electrostatics model rigorously, numerical solution of the finite-difference PB equation is expensive for macromolecular applications. Several approaches for describing electrostatic solvation have been explored in biomolecular modeling as an efficient approximation to numerical solution of the PB equation, at much reduced computational cost. These include empirical models[28,46−49] based on the exposed surface area or volume of the solute complemented with a distance dependent dielectric and ionic side-chain neutralization to compensate for the omitted solvent screening of charge interactions, and continuum electrostatics models,[40,50−57] where the solute−solvent electrostatic interactions are approximated using a dielectric continuum with a large dielectric constant for the solvent (ε = 80 for water), while the solute atomic partial charges are embedded in a dielectric cavity of a small dielectric constant (typically ε = 2−4). The common Generalized Born (GB)[58] continuum methods, which are inspired by the Born equation to compute solvation energies of ions,[59] depend on the determination of effective Born radii that quantify the degree of burial of individual charges within the macromolecule. Analytically solving the Poisson or Poisson−Boltzmann for nonvanishing ionic strength equations[60,61] also falls under this category.[41,62]

In addition to the electrostatic energy contributions, IS methods usually include a nonpolar energy term that accounts for the entropic costs for water to be in contact with the surface of a solute. In touch with the surface of a solute, a water molecule can no longer adopt as many different hydrogen-bond patterns as in bulk water. Together with a loss of entropy of these water molecules, this creates the hydrophobic effect.[18,63,64] The nonpolar contribution to the solvation free energy has two main ingredients. The first term, which represents favorable van der Waals attractions between the solute and solvent molecules, is weak in nature. It depends only on the atomic composition of the solute and can be treated using Weeks−Chandler−Andersen (WCA)-like attractive integral-based methods.[65] The second term represents the cost of breaking the structure of the solvent (water) around the solute, i.e., the cost of cavity formation, which is repulsive in nature and is proportional to solvent-accessible surface area.[66,67] These two terms may be considered separately but are often combined into a single simple term that is assumed to be directly proportional to the solvent accessible surface area scaled by an effective surface tension coefficient.[68]

ES simulations on $A\beta_{13-26}$[7,11] were performed using the CHARMM22/CMAP all-hydrogen force field.[69,70] In the present study, we are also considering the CHARMM19 polar hydrogen force field[71] for the sake of completeness and comparison of force fields. We have categorized the implicit solvation models based on which force field (FF) they are using. The IS models ACE2,[50] ASPENR,[48] EEF1.1,[47] GBORN,[51] and SASA[28] use the CHARMM19 FF, whereas

dx.doi.org/10.1021/ct300941v | J. Chem. Theory Comput. 2013, 9, 834−846

Table 1. Summary of the Implicit Solvent Models Using CHARMM19 Force Field

	ACE2[50]	ASPENR[a,48,73]	EEF1.1[47]	GBORN[51]	SASA[b,28]
	Gaussian charge distribution (not point charges), dielectric boundary: overlapping Gaussian	free energy cost of burring atom	neutralizing ionic side-chains, distance dependent dielectric	extended approach atomic GB radii, scaled vdW radii, dielectric boundary: overlapping spheres	neutralizing ionic side-chains, distance dependent dielectric
polar contribution	GB formalism	~ASP and SASA[c]	Gaussian solvent-exclusion model	parametrized GB formalism	~SASA, free energy cost of burying charges
nonpolar contribution	approximately by pairwise potential	~SASA		~SASA	~SASA

[a]Two sets of atomic solvation parameter and radii: (i) Kyte and Doolittle, (ii) Sharp. [b]Two sets of radii, probabilistic parameters, and connectivity for surface definition: (i) Ferrara, (ii) Haberthuer. [c]Solvent Accessible Surface Area.

Table 2. Summary of the Implicit Solvent Models Using CHARMM22/CMAP Force Field

	FACTS[55]	GBMV II[53]	GBSW[52]	SCPISM[49]	RUSH[72]
	solvent displacement by neighboring solute atoms	dielectric boundary: molecular surface, analytical volume integral method	smoothed dielectric boundary: vdW surface, volume integral method	nonlinear, sigmoidal distance dependent dielectric	employs solute−solvent hydrogen bonding, distance dependent dielectric
polar contribution	GB formalism	GB formalism	GB formalism	parametrized GB formalism	free energy cost of burying hydrogen bond donor/acceptor
nonpolar contribution	~SASA[a]	~SASA	~SASA	~SASA	~SASA

[a]Solvent Accessible Surface Area.

FACTS,[55] GBMV II,[53] GBSW,[52] SCPISM,[49] and RUSH[72] use the CHARMM22/CMAP FF.[69,70] The specifics of each implicit solvent model are fully documented in the original articles. Here, we summarize the key implementation points for each IS model in Tables 1 and 2. Two sets of atomic solvation parameter and radii based on the Wolfenden water to vapor data exist in ASPENR and have been considered in the present study: (1) Values adjusted for the standard state by Kyte and Doolittle (KD)[48] and (2) values as corrected by Sharp (SHARP).[73] In the case of SASA, two sets of radii, probabilistic parameters, and connectivity for surface definition have been taken into consideration: (1) surface-tension like solvation parameters adjusted for the EEF1-modified CHARMM19 parameter set by Ferrara with the original Hasel and Still surface parameters (FER)[28] and (2) the new set of surface parameters (radii, probabilistic parameters, and connectivity parameters) derived in 2002 by Haberthuer, to give a better correlation with exact analytical surfaces than the original Hasel and Still surface parameters (HAB).[28] For the Generalized Born model using molecular volume,[54] we used the analytical method (GBMV II).[53]

ACE2 yields reasonably stable simulations when using CHARMM19 FF and is unreliable with CHARMM22/CMAP FF; therefore we considered using it with CHARMM19.[50] In the case of GBORN[51] and EEF1.1,[47] parameter sets are available for both force fields (albeit not extensively tested with CHARMM22/CMAP for EEF1.1); however we considered using them with CHARMM19 FF because of the computational efficiency. FACTS[55] has been parametrized for protein atoms in both force fields. Since it is only four times slower than vacuum calculation[55] and we can afford to use it with all-hydrogen parameters, we decided to consider FACTS with CHARMM22/CMAP FF.

Preparation of Aβ and Its Mutants. $A\beta_{13-26}$ adopts an α-helical conformation in the membrane environment;[74−76] therefore the initial model structure of $A\beta_{13-26}$ was built in an α-helical conformation in our previous simulation studies.[7,11] Since $A\beta_{13-26}$-WT (HHQKLVFFAEDVGS) is a fragment of the full peptide, the N- and C-termini have been made neutral by capping with N-terminal acetyl and C-terminal amide groups, respectively, mimicking the uncharged amide linkage on both ends of $A\beta_{13-26}$ in the full length peptide. Mutant forms of $A\beta_{13-26}$ were built by modifying wild-type $A\beta_{13-26}$ ($A\beta_{13-26}$-WT) with V18A/F19A/F20A ($A\beta_{13-26}$-MA) and V18L/F19L/F20L ($A\beta_{13-26}$-ML) substitutions. The peptides were built with the ionizable residues in their charged states, where basic residues (H13, H14, and K16) are protonated and acidic residues (E22 and D23) are deprotonated.[11] Thus, the total charge on each model is +1e.

Preparation of the Ligands. The structures of $A\beta_{13-26}$-WT with Dec-DETA ($A\beta_{13-26}$-WT_Dec-DETA) and with Pep1b ($A\beta_{13-26}$-WT_Pep1b) were built using the Insight II program, version 2000 (Figure 1).[11,77] The $A\beta_{13-26}$-WT_Dec-DETA complex is designed such that potential electrostatic interaction with E22 and D23 of $A\beta_{13-26}$-WT is via two basic functional groups (N2 and N3) of Dec-DETA, and potential van der Waals interaction with L17, V18, and A21 of $A\beta_{13-26}$-WT is via the hydrocarbon tail (C1−C9) of Dec-DETA (Figure 1A). For the $A\beta_{13-26}$-WT_Pep1b complex, potential electrostatic interaction with E22 and D23 of $A\beta_{13-26}$-WT is via two basic functional groups (N7/N8 and N5) of Pep1b, potential electrostatic interaction with H13 and K16 of $A\beta_{13-26}$-WT is via two acidic functional groups (O2 and O2/O4/O5) of Pep1b, and potential van der Waals interaction with F20 of $A\beta_{13-26}$-WT is via the indole group of Pep1b (Figure 1B). Ionizable functional groups of Dec-DETA and Pep1b are prepared in their charged states. Thus, the total charges of $A\beta_{13-26}$-WT_Dec-DETA and $A\beta_{13-26}$-WT_Pep1b complexes are +3e and +1e, respectively (Figure 1).

CHARMM22/CMAP or CHARMM19 FF parameters were used, as pertinent for the different IS models. The ligands are peptidomimetic and are designed using amino acid moieties, and therefore ligands can be used without any problem with different implicit solvent models. For both ligands, parameters are given in Tables S1−S6 of Supporting Information.

Molecular Dynamics Simulation. Simulations are performed at 300, 330, 360, and 400 K for wild type $A\beta_{13-26}$. The temperature in each simulation was maintained by coupling all atoms to a Langevin heat bath with frictional coefficient

Table 3. Simulation Conditions and Parameters for CHARMM19 Force Field Based IS Models

	ACE2[50]	ASPENR (KD)[48]	ASPENR (SHARP)[73]	EEF1.1[47]	GBORN[51]	SASA (FER)[28]	SASA (HAB)[28]
ctonnb/ctofnb/cutnb (Å)	8.0/12.0/13.0	10.0/12.0/14.0	10.0/12.0/14.0	7.0/9.0/10.0	10.0/12.0/14.0	6.5/7.5/8.0	6.5/7.5/8.0
cutoff specifications	ATOM[a] SWITCH[b]	ATOM SHIFT[c]	ATOM SHIFT	GROUP[a] SWITCH	ATOM SWITCH	ATOM SHIFT	ATOM SHIFT
solute dielectric	1	1	1	1	1	2	2
solvent dielectric	80				80		
surface tension coeff. (cal/mol.Å^2)	2.5	default (vap_to_wat_kd)	default (vap_to_wat_honig)	default (solvpar)	5	default	default
screening of solute charges	solvent dielectric	solvent dielectric	solvent dielectric	distance dependent dielectric	solvent dielectric	distance dependent dielectric	distance dependent dielectric
remark		no ASP for hydrogens	no ASP for hydrogens	ionic side-chains are neutralized		ionic side-chains are neutralized, solvation of explicit hydrogen atoms is neglected	ionic side-chains are neutralized, solvation of explicit hydrogen atoms is neglected

[a]Electrostatics interactions are computed on an atom−atom pair or group basis. [b]Switch smoothing function for electrostatic calculations from ctonnb to ctofnb. [c]Shift smoothing potential acting to ctofnb and zero beyond.

Table 4. Simulation Conditions and Parameters for CHARMM22/CMAP Force Field Based IS Models

	FACTS[55]	GBMV II[53]	GBSW[52]	SCPISM[49]	RUSH[72]
ctonnb/ctofnb/cutnb (Å)	10.0/12.0/14.0	16.0/18.8/21.0	16.0/16.0/20.0	10.0/12.0/14.0	4.9/5.0/6.0
cutoff specifications	ATOM SHIFT	ATOM SWITCH	ATOM SWITCH	ATOM SHIFT	ATOM SWITCH
solute dielectric	1	1	1	1	1
solvent dielectric	78.5	80	80		
surface tension coeff. (cal/mol Å^2)	15	25	5	5.2	0.72 cal/mol A$^{7/2}$
screening of solute charges	solvent dielectric	solvent dielectric	solvent dielectric	distance dependent dielectric	distance dependent dielectric
remark	factor in the denominator of exponential function in generalized Born formula is taken 8.0.	factor in the denominator of exponential function in generalized Born formula is taken 8.0; analytical molecular volume integration	optimized Born radii[87] (radius_gbsw) used; improved Coulomb field approx., volume integration method	SCPISM parameter set (scpism) used.	employs solute−solvent hydrogen bond; free energy cost of burying H-bond donor/acceptor

dx.doi.org/10.1021/ct300941v | J. Chem. Theory Comput. 2013, 9, 834−846

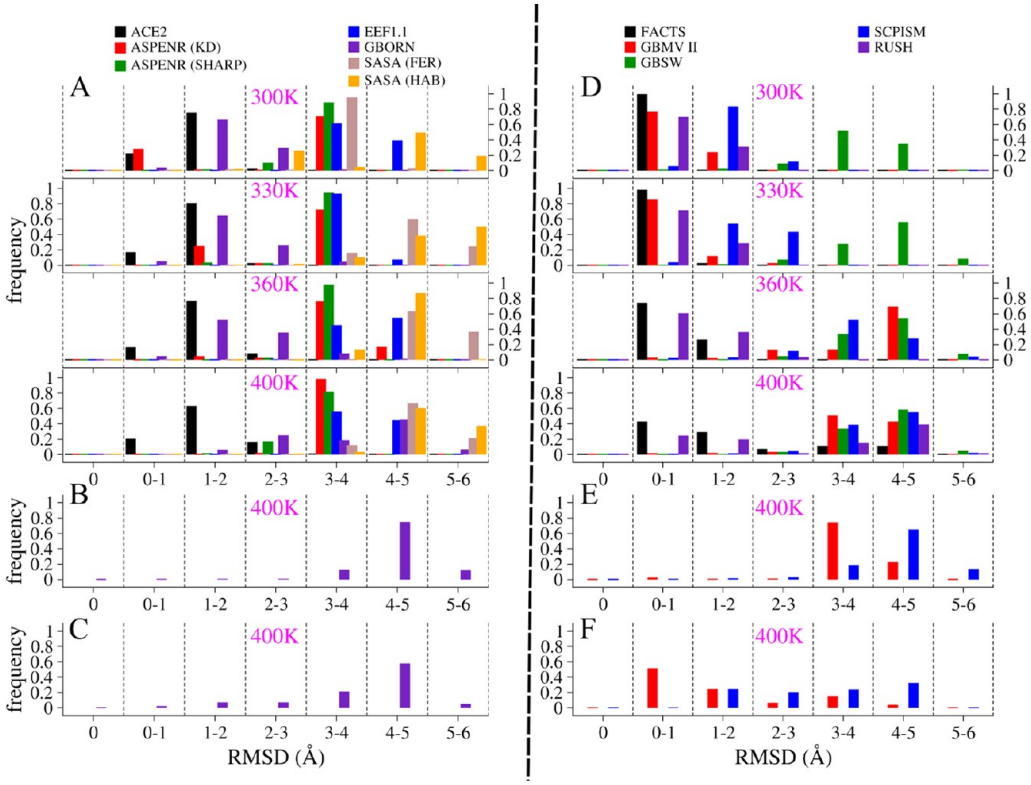

Figure 2. Distribution of backbone heavy atoms' RMSD of Aβ_{13-26} middle region (15−24) using CHARMM19 FF based IS models: (A) Aβ_{13-26}-WT at 300, 330, 360, and 400 K; (B) Aβ_{13-26}-MA at 400 K; (C) Aβ_{13-26}-ML at 400 K; and CHARMM 22/CMAP FF based IS models: (D) Aβ_{13-26}-WT at 300, 330, 360, and 400 K; (E) Aβ_{13-26}-MA at 400 K; (F) Aβ_{13-26}-ML at 400 K.

β = 2 ps^{-1}.[78] All simulations and analyses were carried out using CHARMM[79,80] version c36a6 with the CHARMM22/CMAP all-hydrogen FF[69,70] for FACTS,[55] GBMV II,[53] GBSW,[52] SCPISM,[49] and RUSH[72] and with the CHARMM19 polar hydrogen FF for ACE2,[50] ASPENR,[48] EEF1.1,[47] GBORN,[51] and SASA.[28] The SHAKE algorithm[81] was used to fix the length of the covalent bonds involving hydrogen atoms, allowing an integration time step of 2 fs to be used in the integration of Newton's equations. The simulation parameters specific to each IS model are listed in Tables 3 and 4. All calculations were performed on a GNU/Linux PC cluster with 64 bit Intel Xeon and AMD processors.

Before the simulations of wild-type Aβ_{13-26}, structures of respective models were optimized by 2000 steps of steepest descent followed by 4000 steps of adopted basis Newton−Raphson. The system was heated up to the target temperature (300, 330, 360, or 400 K) gradually for 20 ps employing velocity rescaling. The system was then shifted to a Langevin heat bath of respective temperature and equilibrated for 30 ps. After equilibration, production runs of 100 ns were carried out with a coordinates saving frequency of 1 ps. The simulations of both mutants and Aβ_{13-26} with ligands used the same parameters and conditions, except that simulations were carried out only at 400 K.

Analysis. Every snapshot (1 ps) of the production run (100 ns) was analyzed except as otherwise stated. To probe the unfolding of wild-type Aβ_{13-26} and the effect of mutations, the root-mean-square deviation (RMSD) was computed for the middle region (15−24) of Aβ_{13-26} and thus avoided large fluctuations originating from mobile N- and C-termini. RMSD was calculated for the backbone heavy atoms against the initial energy-minimized coordinates along the MD simulation.

For the conformational patterns of Aβ_{13-26} observed during the simulations, we calculated the number of α-helical backbone hydrogen bonds (αHBs), as well as the helicity based on backbone torsion angles (Φ, Ψ) and on the Kabsch−Sander DSSP algorithm.[82] Hydrogen bonds were defined using a criterion acceptor−hydrogen distance < 2.4 Å.[83] For torsion angle based helicity analysis, the results are reported as the fraction of the 10 torsion angle (Φ, Ψ) pairs in the middle region (15−24) of Aβ_{13-26} that are in the α-helical region ($-89 \leq \Phi \leq -39$ and $-66 \leq \Psi \leq -16$).[84]

To examine the effect of ligands on the structural changes in Aβ_{13-26}, the RMSD, αHB count, and helicity of the residues 15−24 of Aβ_{13-26} were calculated in the presence of ligands. To probe the ligands' interactions with Aβ_{13-26}-WT, we employed similar criteria from our previous study.[11] On the basis of the distances measured for the initial energy-minimized structures of Aβ_{13-26}-WT and ligand complexes, a contact between Aβ_{13-26}-WT and the ligand was counted for distances < 6.0 Å. Polar contacts were determined by counting the number of hydrogen bonds between Aβ_{13-26}-WT and ligands. Nonpolar interactions were determined considering C−C and C−N contacts using distances < 5.0 Å, extracted from vdW radii of carbon, nitrogen, and hydrogen, and C−H and N−H covalent bond lengths. Ligands are designed to have nonpolar interactions between backbone and side chain carbon atoms (excluding backbone carbonyl carbons) of Aβ_{13-26}-WT middle nonpolar residues ($L_{17}VFFA_{21}$) and nonpolar heavy atoms of the ligand (hydrocarbon tail (C_1−C_9) of Dec-DETA or indole group (C_{13}−C_{20} and N_3) of Pep1b). At least one polar or one nonpolar contact has to be present for the ligand to be

dx.doi.org/10.1021/ct300941v | J. Chem. Theory Comput. 2013, 9, 834−846

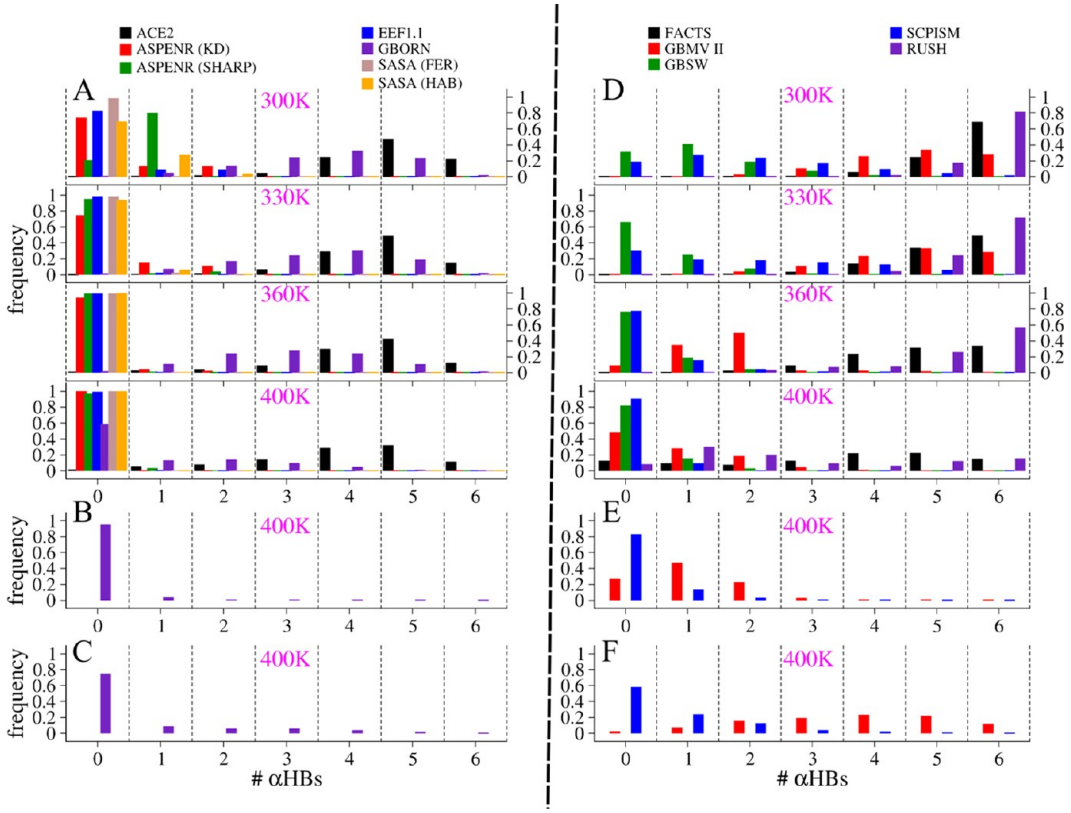

Figure 3. Distribution of number of αHBs in the middle region (15−24) of Aβ_{13-26} using CHARMM19 FF based IS models: (A) Aβ_{13-26}-WT at 300, 330, 360, and 400 K; (B) Aβ_{13-26}-MA at 400 K; (C) Aβ_{13-26}-ML at 400 K; and CHARMM 22/CMAP FF based IS models: (D) Aβ_{13-26}-WT at 300, 330, 360, and 400 K; (E) Aβ_{13-26}-MA at 400 K; (F) Aβ_{13-26}-ML at 400 K.

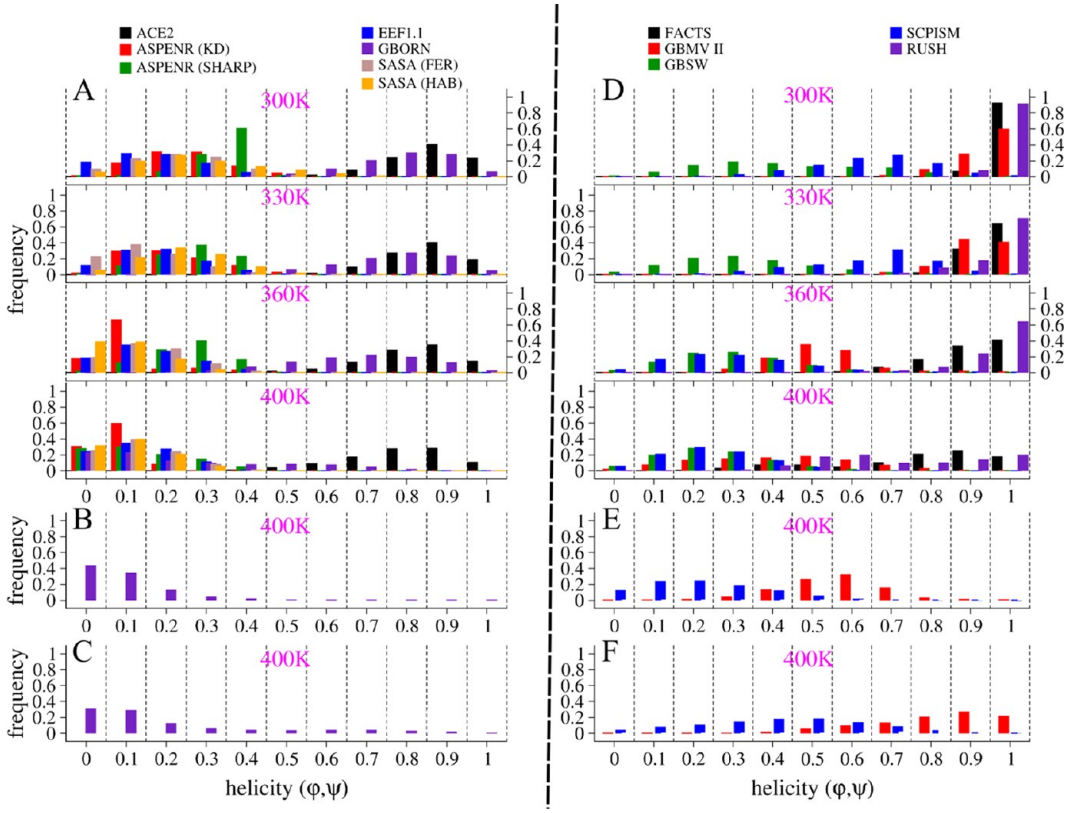

Figure 4. Distribution of the helicity of Aβ_{13-26} middle region (15−24) considering 10 torsion angle (Φ, Ψ) pairs using CHARMM19 FF based IS models: (A) Aβ_{13-26}-WT at 300, 330, 360, and 400 K; (B) Aβ_{13-26}-MA at 400 K; (C) Aβ_{13-26}-ML at 400 K; and CHARMM 22/CMAP FF based IS models: (D) Aβ_{13-26}-WT at 300, 330, 360, and 400 K; (E) Aβ_{13-26}-MA at 400 K; (F) Aβ_{13-26}-ML at 400 K.

dx.doi.org/10.1021/ct300941v | J. Chem. Theory Comput. 2013, 9, 834−846

Table 5. Performance of IS Models Classified to Different Groups[a] Based on the RMSD, αHB Count, and Helicity of the Middle Region (15-24) of $A\beta_{13-26}$ Conformers Generated in the Simulations Employing Different IS Models on the $A\beta_{13-26}$ Wild-Type, Its Mutants, and the $A\beta_{13-26}$ Wild-Type in Presence of Ligands at Different Temperatures

		$A\beta_{13-26}$-WT				$A\beta_{13-26}$-MA	$A\beta_{13-26}$-ML	$A\beta_{13-26}$-WT with Dec-DETA	$A\beta_{13-26}$-WT with Pep1b
FF	IS model/temp.	300 K	330 K	360 K	400 K	400 K	400 K	400 K	400 K
CHARMM19	ACE2	A	A	A	A				
	ASPENR (KD)	C	C	C	C				
	ASPENR (SHARP)	C	C	C	C				
	EEF1.1	C	C	C	C				
	GBORN	A	A	B	C	C	C		
	$GBORN_{QP}$							B	B
	SASA (FER)	C	C	C	C				
	SASA (HAB)	C	C	C	C				
CHARMM22/CMAP	FACTS	A	A	A	A				
	GBMV II	A	A	B	C	B	A	A	A
	GBSW	C	C	C	C				
	SCPISM	A	B	C	C	C	B	C	C
	RUSH	A	A	A	A				

[a]Group A (folded): RMSD < 2 Å, 2 ≤ αHBs ≤ 6, and 60% ≤ helicity ≤ 100%. Group B (moderately unfolded): RMSD ≥ 2 Å, 1 ≤ αHBs ≤ 4, and 40% ≤ helicity ≤ 80%. Group C (highly unfolded): RMSD ≥ 4 Å, αHBs ≈ 0, and helicity ≤ 40%.

considered bound to $A\beta_{13-26}$-WT. The orientation of the ligand bound to $A\beta_{13-26}$-WT is determined by the angle between the end-to-end vector of the ligand (C_1-N_3 of Dec-DETA or C_4-C_{22} of Pep1b) and that of $A\beta_{13-26}$-WT (aliphatic carbon of acetylated N-terminus and amide nitrogen of amidated C-terminus).

Pair-wise RMSDs of backbone heavy atoms of residues 15−24 of $A\beta_{13-26}$ were calculated between all coordinate pairs every 100 ps from the production run, which were then projected onto a 2D plane for the clustering of conformers.[85,86] This Sammon mapping, or 2D projection, of the RMSD matrix assigns a point (P_i, Q_i) to each conformer i, such that the distances between all pairs of points, (P_i, Q_i) and (P_j, Q_j), are optimally close to the corresponding RMSDs between conformers i and j.

RESULTS AND DISCUSSION

Aβ Unfolding. To examine the temperature at which $A\beta_{13-26}$ unfolds, simulations were performed at 300, 330, 360, and 400 K. Following our previous study,[7] the performance of IS models has been classified into three groups (A, B, and C) based on the conformers of the middle region (15−24) generated during the simulation: Group A (folded) with RMSD < 2 Å, 2 ≤ αHBs ≤ 6, and 60% ≤ helicity ≤ 100%. Group B (moderately unfolded) with RMSD ≥ 2 Å, 1 ≤ αHBs ≤ 4, and 40% ≤ helicity ≤ 80%. Group C (highly unfolded) with RMSD ≥ 4 Å, αHBs ≈ 0, and helicity ≤ 40%.

CHARMM19 FF Based IS Models. $A\beta_{13-26}$ was found to be unfolded irrespective of temperature using either of the IS models: ASPENR(KD), ASPENR(SHARP), EEF1.1, SASA-(FER), and SASA(HAB), where RMSD ≥ 3 Å (Figure 2A), αHBs ≈ 0 (Figure 3A), and helicity ≤40% (Figure 4A and S1A) was observed. Thus, these models fall in group C at all four temperatures. Whereas with ACE2, a majority of conformers had a RMSD < 2 Å (Figure 2A), an αHB count in the range 2−6 (Figure 3A), and a helicity 60−100% (Figure 4A and S1A), satisfying the criteria of being in group A at all four temperatures, which indicates overstabilization of the helix irrespective of temperature. It was only with GBORN that the trend of increase in RMSD (Figure 2A), decrease in αHB count

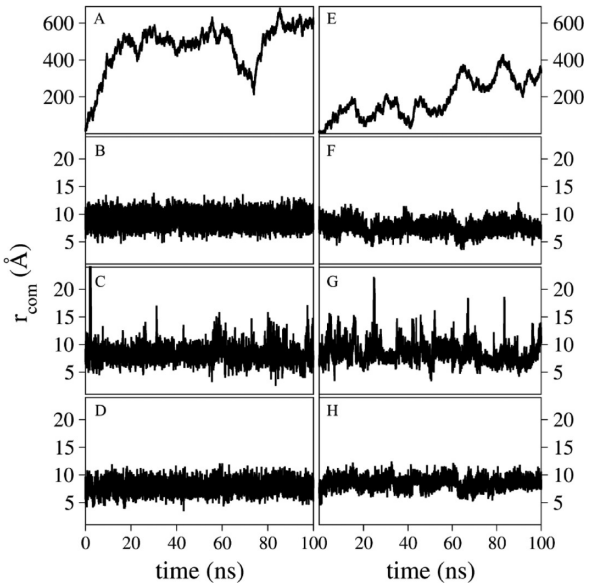

Figure 5. Center of mass distance between $A\beta_{13-26}$-WT and the ligand at 400 K. $A\beta_{13-26}$-WT with Dec-DETA using (A) GBORN, (B) $GBORN_{QP}$, (C) GBMV II, and (D) SCPISM and $A\beta_{13-26}$-WT with Pep1b using (E) GBORN, (F) $GBORN_{QP}$, (G) GBMV II, and (H) SCPISM.

(Figure 3A), and decrease in helicity (Figure 4A and S1A) was observed with increasing temperature. Melting of the helix was visible as the temperature reached 360 K and became more prominent at 400 K. The categorization of IS models at different temperatures has been summarized in Table 5.

CHARMM22/CMAP FF Based IS Models. Employing FACTS and RUSH, the distributions mostly had a RMSD < 2 Å (Figure 2D), an αHB count ranging 2−6 (Figure 3D), and a helicity of 60−100% (Figure 4D and S1D), satisfying the criteria of being in group A at all four temperatures, indicating overstabilization of the helix irrespective of temperature. Using GBSW, a majority of conformers had a RMSD ≥ 3 Å (Figure 2D), αHBs ≈ 1 (Figure 3D), and a helicity ≤ 40% (Figure 4D and S1D) irrespective of the temperature, indicating the helix to be

dx.doi.org/10.1021/ct300941v | J. Chem. Theory Comput. 2013, 9, 834−846

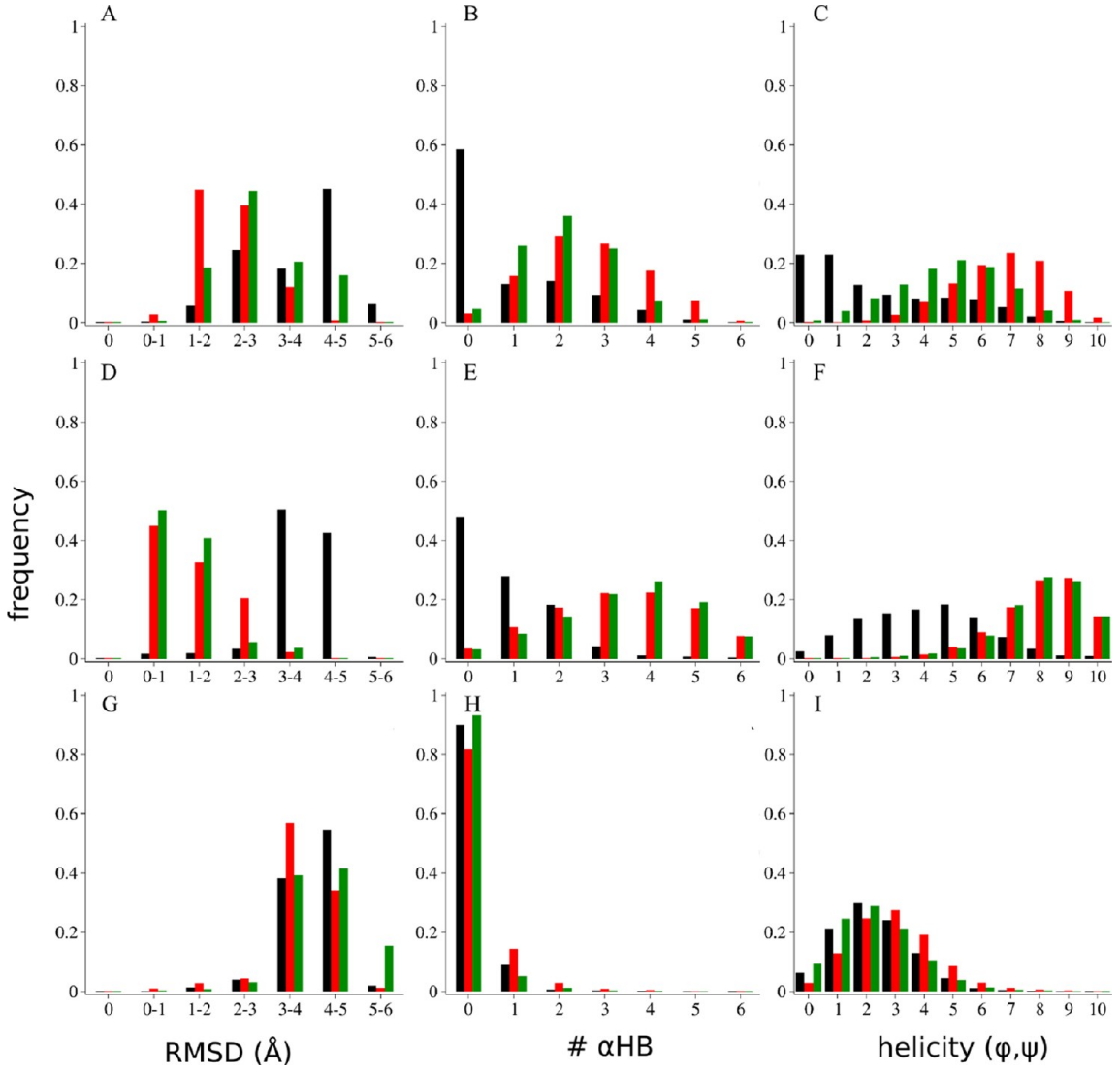

Figure 6. Distribution of the number of αHBs and backbone heavy atoms' RMSD and helicity of the Aβ_{13-26} middle region (15−24) at 400 K in Aβ_{13-26}-WT alone (black), Aβ_{13-26}-WT with Dec-DETA (red), and Aβ_{13-26}-WT with Pep1b (green) using GBORN$_{QP}$ (A−C), GBMV II (D−F), and SCPISM (G−I).

unfolded and thus classifying GBSW in group C at all four temperatures. Using SCPISM, melting of the helix was observed. At 300 K, the helix was folded; it partially unfolded at 330 K and completely unfolded as the temperature reached 360 K. At 400 K, distributions having a RMSD $\geq$ 3 Å (Figure 2D), αHBs $\approx$ 0 (Figure 3D), and a helicity $\leq$ 40% (Figure 4D) were observed. Similar trends of unfolding were also observed when GBMV II was employed, where up to 330 K the helix was folded, with unfolding occurring at 360 K. Distributions having a RMSD $\geq$ 3 Å (Figure 2D), αHBs $\approx$ 0 (Figure 3D), and a helicity $\leq$ 40% (Figure 4D) were observed at 400 K. The categorization of IS models at different temperatures has been summarized in Table 5.

Effects of Mutations. Aβ_{13-26}-WT was completely unfolded at 400 K employing GBORN, GBMV II, and SCPISM; thus these IS models were taken further to investigate their ability to reproduce the stabilizing effect of mutations on the Aβ_{13-26} helix. For this, mutant models with alanine (Aβ_{13-26}-MA) and leucine (Aβ_{13-26}-ML) were simulated at 400 K. Here also, the performance of IS models has been classified into three groups (Table 5) based on the criteria mentioned above.

GBORN was categorized as group C, when employed on either of the mutants, since distributions mostly had a RMSD $\geq$ 4 Å (Figure 2B and C), αHBs $\approx$ 0 (Figure 3B and C), and helicity $\leq$ 40% (Figure 4B,C and S1B,C). Employing GBMV II on Aβ_{13-26}-MA, the helix was moderately unfolded (group B), as distributions mostly has a RMSD ranging 3−4 Å (Figure 2E), αHBs $\leq$ 2 (Figure 3E), and 40% $\leq$ helicity $\leq$ 80% (Figure 4E). While using GBMV II on Aβ_{13-26}-ML, the helix was folded (group A), since a majority of conformers had a RMSD < 2 Å (Figure 2F), 2−6 αHBs (Figure 3F), and 50−100% helicity (Figure 4F). With SCPISM on Aβ_{13-26}-MA, the helix unfolded almost completely (group C) since distributions mostly had a RMSD $\geq$ 4 Å (Figure 2E), αHBs $\approx$ 0 (Figure 3E), and helicity $\leq$ 40% (Figure 4E and S1E). SCPISM on Aβ_{13-26}-ML produced moderate unfolding of the helix (group B) as a majority of conformers had RMSD 2−5 Å (Figure 2F), αHBs $\leq$ 4 (Figure 3F), and helicity 10−80% (Figure 4F).

Effects of Ligands on the Stability of Aβ_{13-26}. Here also we considered GBORN, GBMV II, and SCPISM to evaluate

dx.doi.org/10.1021/ct300941v | J. Chem. Theory Comput. 2013, 9, 834−846

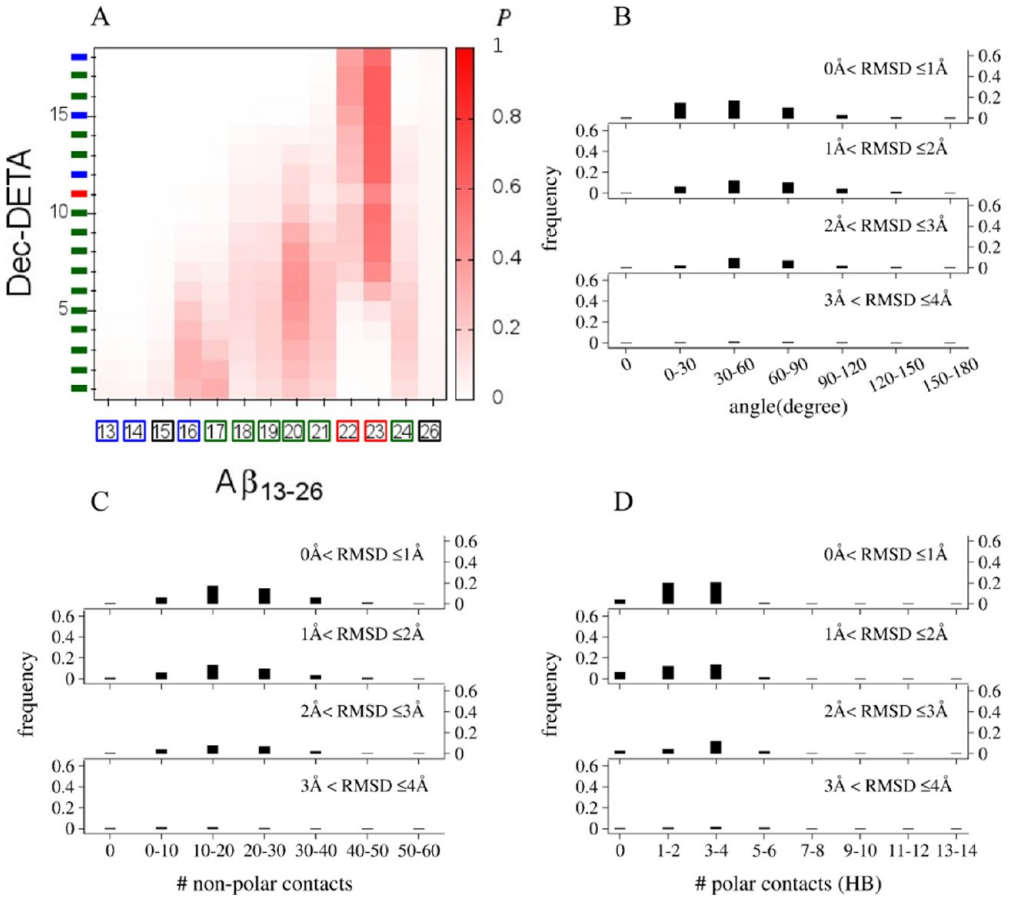

Figure 7. Contact map, angle distribution, nonpolar and polar contacts between Aβ_{13-26}-WT and Dec-DETA using GBMV II at 400 K. (A) The contact probability between the center of geometry of side chain heavy atoms of each residue of Aβ_{13-26}-WT and each heavy atom of Dec-DETA, which ranges from 0 (white) representing no contacts to 1 (red) representing all contacts throughout simulation. Numbers in boxes on the *X* axis represent basic (blue), acidic (red), nonpolar (green), and uncharged-polar (black) residues of Aβ_{13-26}-WT. The numbers on the *Y* axis represent carbon (green), nitrogen (blue), and oxygen (red) atoms of Dec-DETA. Also shown is a distribution of Aβ_{-13-26}-WT, considering (B) the angle between end-to-end vectors of Aβ_{13-26}-WT and of Dec-DETA, (C) the number of nonpolar (NP) contacts, and (D) the number of polar contacts, i.e., the number of hydrogen bonds (HB).

their efficacy concerning the stability of Aβ_{13-26} in the presence of ligands (Figure 1) at 400 K. The performance of IS models has been classified into three groups (Table 5) based on the criteria mentioned above. In the case of GBORN with either of the ligands, the ligand dissociates at the very beginning (Figure 5A, E). In order to keep the ligand from escaping the vicinity of Aβ_{13-26}-WT, a mass-weighted quartic droplet potential was applied with a force constant of 1.4×10^{-6} kcal mol^{-1} Å^{-4}, which presents an initially flat restraint energy that for ligand carbons reaches 1 kcal mol^{-1} at 15 Å from the system center of mass. GBORN with the quartic droplet potential was termed GBORN$_{QP}$ and ligands remained close to the Aβ_{13-26}-WT (Figure 5B, F). Using GBORN$_{QP}$ on Aβ_{13-26}-WT with either of the ligands, a moderately unfolded helix (group B) was obtained, where the probability of unfolding was greater with Pep1b than with Dec-DETA. Also the probabilities of polar and nonpolar contacts between Aβ_{13-26}-WT and either of the ligands were medium (Figure S2A, C). For Aβ_{13-26}-WT with Dec-DETA, a majority of conformers had 1−3 Å RMSD (Figure 6A), 1−4 αHBs (Figure 6B), and 40−80% helicity (Figure 6C), while for Aβ_{13-26}-WT with Pep1b, the distributions were with a RMSD ranging 1−5 Å (Figure 6A), αHBs 1−3 (Figure 6B), and helicity 20−70% (Figure 6C).

Employing GBMV II on Aβ_{13-26}-WT with either of the ligands, the ligand remained close to Aβ_{13-26}-WT (Figure 5C, G), and a folded helix was obtained (group A), since distributions mostly had a RMSD < 2 Å (Figure 6D), αHBs 2−6 (Figure 6E), and helicity 60−100% (Figure 6F). In this case, the probabilities of polar and nonpolar contacts between Aβ_{13-26}-WT and either of the ligands were high (Figures 7A and 8A). These contacts are important for the stability of Aβ_{13-26}, as reported in our previous study[11] and experimentally.[10] Using SCPISM on Aβ_{13-26}-WT with either of the ligands, even though the ligands remained close to Aβ_{13-26}-WT (Figure 5D, H), the helix unfolded (group C) because conformers had a RMSD ≥ 3 Å (Figure 6G), αHBs ≈ 0 (Figure 6H), and helicity ≤ 40% (Figure 6I). It was found that the probabilities of polar contacts was medium, and that of nonpolar contacts was low between Aβ_{13-26}-WT and Dec-DETA (Figure S2B), and for Pep1b the probabilities were lower for both polar and nonpolar contacts (Figure S2D).

Comparison of GBMV II and ES Models. The stabilizing effect of ligands on the Aβ_{13-26}-WT helix was clearly seen only with GBMV II at 400 K. The contact probabilities between Aβ_{13-26}-WT and Dec-DETA (Figure 7A) and Pep1b (Figure 8A) are similar to the ones reported in ES simulations (see Figures 4 and 5 of Ito et al.[11]), i.e. higher contact probabilities between

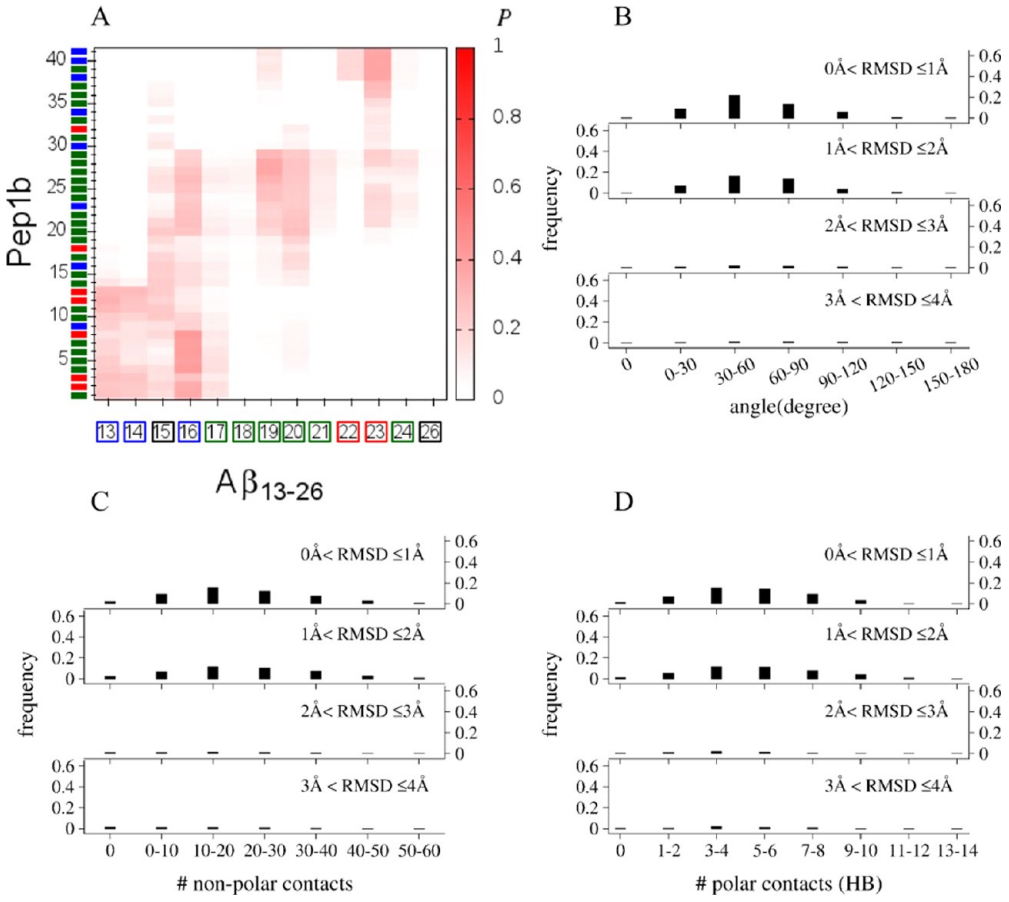

Figure 8. Contact map, angle distribution, nonpolar and polar contacts between Aβ_{13-26}-WT and Pep1b using GBMV II at 400 K. (A) The contact probability between the center of geometry of side chain heavy atoms of each residue of Aβ_{13-26}-WT and each heavy atom of Pep1b, which ranges from 0 (white) representing no contacts to 1 (red) representing all contacts throughout simulation. Numbers in boxes on the *X* axis represent basic (blue), acidic (red), nonpolar (green), and uncharged-polar (black) residues of Aβ_{13-26}-WT. The numbers on the *Y* axis represent carbon (green), nitrogen (blue), and oxygen (red) atoms of Pep1b. Also shown is the distribution of Aβ_{13-26}-WT, considering (B) the angle between end-to-end vectors of Aβ_{13-26}-WT and of Pep1b, (C) the number of nonpolar (NP) contacts, and (D) the number of polar contacts, i.e., the number of hydrogen bonds (HB).

basic functional groups of ligands and acidic residues (Glu22 and Asp23) of Aβ_{13-26}-WT, medium contact probabilities between acidic functional groups of Pep1b and basic residues (His13 and Lys16) of Aβ_{13-26}-WT, and low nonpolar contact probabilities between Dec-DETA and Aβ_{13-26}-WT residues Leu17 to Ala21 and Pep1b and Aβ_{13-26}-WT residues Phe19 and Phe20. Pep1b had more polar (Figure 8D) and nonpolar (Figure 8C) contacts with Aβ_{13-26}-WT compared to Dec-DETA (Figure 7D,C), in good agreement with ES simulations.[11] This can be related to the design of the ligands where a centrally placed indole group straddles the middle Aβ_{13-26} nonpolar part (residue 17−21), while basic and acidic functional groups of Pep1b simultaneously bind to the acidic and basic residues of Aβ_{13-26}, respectively. The basic functional groups and hydrocarbon tail in Dec-DETA have lower probabilities of these interactions when compared to Pep1b. More contacts in Pep1b were also indicated considering the angle between end-to-end vectors of Aβ_{13-26}-WT and of Pep1b, where the distribution was concentrated in the angle range of 30−60° (Figure 8B), whereas in the case of Dec-DETA, it was extending up to an angle range of 90−120° (Figure 7B), resulting in fewer contacts.

We calculated the pairwise backbone heavy atoms' RMSD of the residues 15−24 of Aβ_{13-26} at every 100 ps of the 100 ns long simulation using GBMV II at 400 K and a 20 ns explicit solvent simulation at 360 K from our previous study.[7,11] The RMSD matrices obtained by using GBMV II for Aβ_{13-26}-WT alone (Figure 9A), Aβ_{13-26}-WT with Dec-DETA (Figure 9B), and Aβ_{13-26}-WT with Pep1b (Figure 9C) were similar to the RMSD matrices obtained by using explicit solvent (Figure 9D, E, and F respectively). With GBMV II, densely packed clusters indicate helical Aβ_{13-26} with Dec-DETA (Figure S3B) and with Pep1b (Figure S3C). These clusters were quite comparable to the ones in the ES simulation (Figure S3E, F respectively). Considering RMSD matrices and clustering, partial and complete helix unfolding were observed with GBORN$_{QP}$ (Figure S4) and SCPISM (Figure S5), respectively.

Efficiency of IS Models. It is of interest to examine the computational efficiency of the IS models, for which we performed 100 ps long simulations of Aβ_{13-26}-WT with every IS model. All the benchmarkings were performed on a 2.40 GHz 64 bit E5645 Intel Xeon processor. Among the CHARMM19 FF based IS models, ASPENR was most expensive, whereas SASA and EEF1.1 were the cheapest, while ACE2 and GBORN came in between (Figure 10A). All models except EEF1.1 and SASA scale quite well with the number of processors (Figure 10A). Among CHARMM22/CMAP FF based IS models, GBMV II was most expensive, and

dx.doi.org/10.1021/ct300941v | J. Chem. Theory Comput. 2013, 9, 834−846

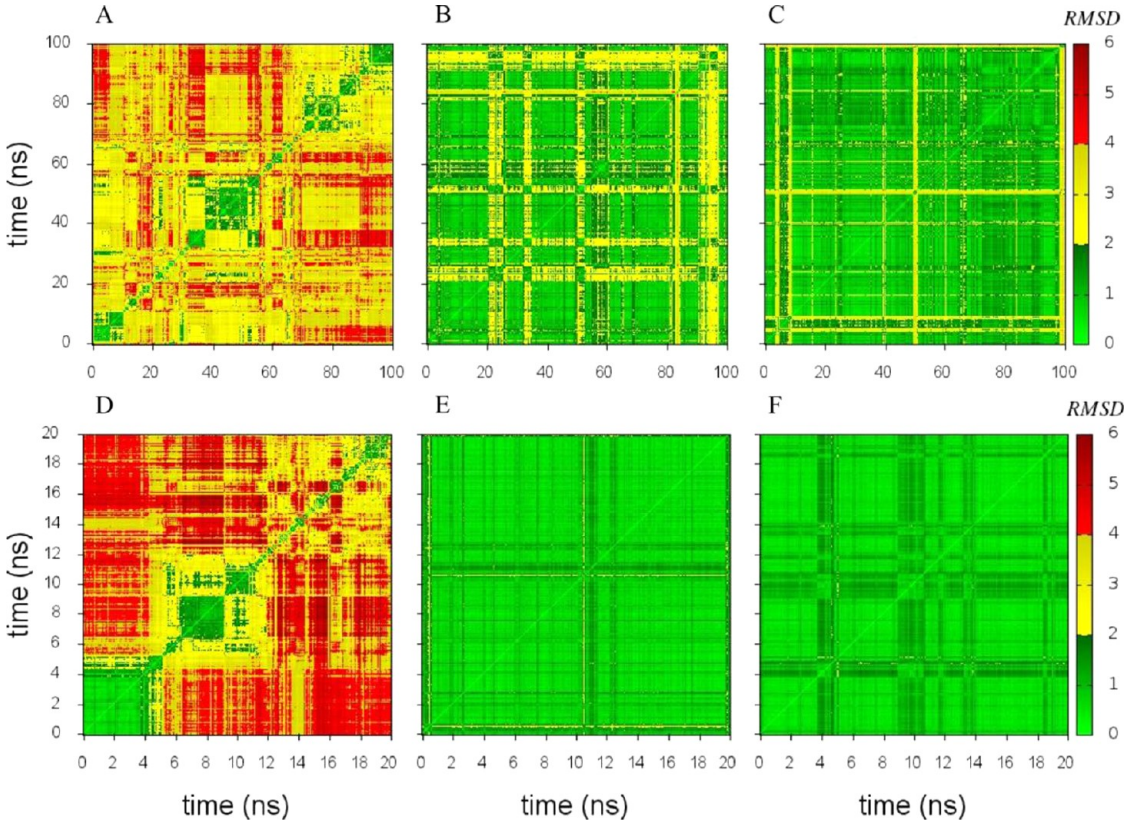

Figure 9. RMSD matrix using the GBMV II model at 400 K and explicit solvent at 360 K. Pair-wise backbone heavy atoms' RMSD of the middle region (15−24) of Aβ_{13-26} conformers at every 100 ps of a 100 ns production run, using GBMV II on (A) Aβ_{13-26}-WT, (B) Aβ_{13-26}-WT with Dec-DETA, and (C) Aβ_{13-26}-WT with Pep1b. Similarly for a 20 ns production run in explicit solvent on (D) Aβ_{13-26}-WT, (E) Aβ_{13-26}-WT with Dec-

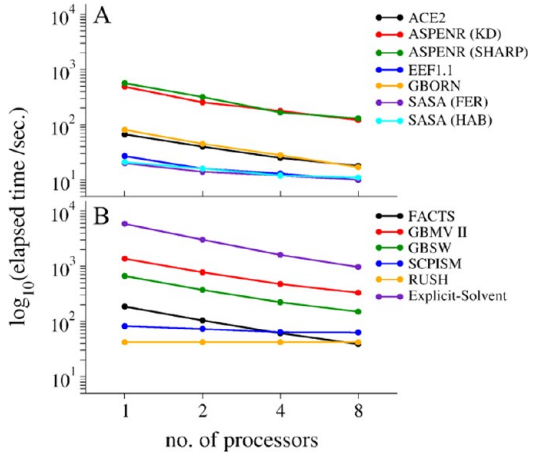

Figure 10. Efficiency of IS models. Elapsed time in running 100 ps simulation of Aβ_{13-26} using (A) CHARMM19 FF based IS models and (B) CHARMM22/CMAP FF based IS.

cheaper than that was GBSW, which was then followed by FACTS, whereas SCPISM and RUSH, both being non-parallelized, were the cheapest (Figure 10B). GBMV II, GBSW, and FACTS scaled nicely with the number of processors (Figure 10B). As expected, the cost of explicit solvent calculations (Figure 10B) of a similar system using the same conditions[7] is much greater than any implicit solvent model. The computational costs (Table 6) on a single processor correlate well with the "intrinsic cost" reported by Brooks et al.[80] apart from GBSW and GBMV II. The reason for

Table 6. Approximate Computational Cost for Each IS Model Relative to a Corresponding Vacuum Calculation in Running a 100 ps Simulation of Aβ_{13-26} on Single Processor

CHARMM19 FF		CHARMM22/CMAP FF	
IS model	cost relative to vacuum	IS models	cost relative to vacuum
ACE2	~3	FACTS	~3.25
ASPENR	~23	GBMV II	~23
EEF1.1	~1.5	GBSW	~10
GBORN	~4	SCPISM	~1.6
SASA	~2	RUSH	~1.6

the higher relative cost of the GBSW and GBMV II in the present study as compared to Brooks et al. is that the performances of these implicit models improve as the system size increases.[52,54]

CONCLUSION

We systematically investigated the efficiency and efficacy of implicit solvent (IS) models to capture the unfolding of wild-type Aβ_{13-26} and its stabilization either by mutations or ligands. Our findings give further insight into the choice of appropriate IS model to study the system of interest. Most IS models generated either unfolded or folded Aβ_{13-26} conformers at all of the temperatures and were not considered in further investigations because of their inability to reflect the unfolding behavior of the helix with increasing temperature. It was only for GBORN, GBMV II, and SCPISM that clear trends of unfolding (completely or partially) were observed, where the

helix was completely unfolded at 400 K, and thus only these three IS models were investigated further.

Considering the ability to stabilize the helical Aβ_{13-26} conformation with the introduction of mutations, among these three IS models GBMV II performed better than the other two. GBORN generated unfolded helices from either of the mutants, whereas with SCPISM, an unfolded and partially unfolded helix was obtained for the alanine and leucine mutant models, respectively. However, with GBMV II, Aβ_{13-26} was partially helical (alanine mutant) or helical Aβ_{13-26} (leucine mutant). Taking into account the last two models (SCPISM and GBMV II), the stabilizing effect of mutations on the Aβ_{13-26} helix is consistent with experimental data for Aβ_{12-28}[5] and simulation data for Aβ_{13-26}[7] and full length Aβ_{1-42}.[6] In addition, we observed that the leucine mutant model stabilizes the helix more than the alanine mutant model.

When accounting for the ability to produce the helical Aβ_{13-26} conformers in the presence of ligands, here again GBMV II performed the best. Even with the application of mass-weighted quartic droplet potential to retain the ligands close to wild-type Aβ_{13-26}, employment of GBORN produced only medium probabilities of polar and nonpolar contacts between Aβ_{13-26} and either of the ligands, which could be the reason for not being able to generate a folded helix. SCPISM generated an unfolded helix with either of the ligands because of its inability to reproduce the polar and nonpolar interactions between Aβ_{13-26} and the ligands. It was only with GBMV II that the increase in the stability of the helix with the presence of either of the ligands was observed, because it qualitatively reproduced polar/nonpolar contacts needed for the binding of the ligand with wild-type Aβ_{13-26} and for the stability of the helix.[10,11] Furthermore, GBMV II showed Aβ_{13-26} having more polar/nonpolar contacts with Pep1b than with Dec-DETA, substantiating Pep1b being more effective in the inhibition of the unfolding of the helix.[11] Our study indicates that GBMV II would be a powerful tool to perform large-scale screening to investigate the effects of various mutations or ligands on the stability of the Aβ central helix, which would assist in rational drug design.

■ ASSOCIATED CONTENT

Supporting Information

Force field parameters for both the ligands, helicity based on hydrogen bond existence, contact maps, and RMSD matrix and cluster. This material is available free of charge via the Internet at http://pubs.acs.org.

■ AUTHOR INFORMATION

Corresponding Author

*Tel.: +46-8-524 81099. Fax: +46-8-524 81135. E-mail: Lennart.Nilsson@ki.se.

Notes

The authors declare no competing financial interest.

■ ACKNOWLEDGMENTS

This work was supported by the Swedish Research Council.

■ ABBREVIATIONS

Aβ, amyloid β-peptide; ES, explicit solvent; FF, force field; GB, generalized Born; IS, implicit solvent; MD, molecular dynamics; RMSD, root-mean-square deviation

■ REFERENCES

(1) Querfurth, H. W.; LaFerla, F. M. *N. Engl. J. Med.* **2010**, *362*, 329−344.
(2) Tjernberg, L. O.; Näslund, J.; Lindqvist, F.; Johansson, J.; Karlström, A. R.; Thyberg, J.; Terenius, L.; Nordstedt, C. *J. Biol. Chem.* **1996**, *271*, 8545−8548.
(3) Caflisch, A. *Curr. Opin. Chem. Biol.* **2006**, *10*, 437−444.
(4) Chiti, F.; Calamai, M.; Taddei, N.; Stefani, M.; Ramponi, G.; Dobson, C. M. *Proc. Natl. Acad. Sci. U. S. A.* **2002**, *99*, 16419−16426.
(5) Päiviö, A.; Nordling, E.; Kallberg, Y.; Thyberg, J.; Johansson, J. *Protein Sci.* **2004**, *13*, 1251−1259.
(6) Nordling, E.; Kallberg, Y.; Johansson, J.; Persson, B. *J. Comput.-Aided Mol. Des.* **2008**, *22*, 53−58.
(7) Ito, M.; Johansson, J.; Strömberg, R.; Nilsson, L. *PLoS ONE* **2011**, *6*, e17587.
(8) Li, J.; Liu, R.; Lam, K. S.; Jin, L.-W.; Duan, Y. *Biophys. J.* **2011**, *100*, 1076−1082.
(9) Convertino, M.; Pellarin, R.; Catto, M.; Carotti, A.; Caflisch, A. *Protein Sci.* **2009**, *18*, 792−800.
(10) Nerelius, C.; Sandegren, A.; Sargsyan, H.; Raunak, R.; Leijonmarck, H.; Chatterjee, U.; Fisahn, A.; Imarisio, S.; Lomas, D. A.; Crowther, D. C.; Strömberg, R.; Johansson, J. *Proc. Natl. Acad. Sci. U. S. A.* **2009**, *106*, 9191−9196.
(11) Ito, M.; Johansson, J.; Strömberg, R.; Nilsson, L. *PLoS ONE* **2012**, *7*, e30510.
(12) Ben-Naim, A. Solvent Effects on Protein Stability and Protein Association. In *Protein-Solvent Interactions*, 1st ed.; Gregory, R. B., Ed.; Marcel Dekker, Inc.: New York, 1995; Vol. *592*, pp 387−420.
(13) *Water: A Comprehensive Treatise*; Franks, F., Ed.; Plenum Pub Corp: New York, 1972−1982; Vol. *1*−*7*.
(14) Eisenberg, D.; McLachlan, A. D. *Nature* **1986**, *319*, 199−203.
(15) Honig, B.; Yang, A.-S. Free Energy Balance in Protein Folding. In *Adv. Protein Chem.*; Anfinsen, C. B., Richards, F. M., Edsall, J. T., Eisenberg, D. S., Eds.; Academic Press: San Diego, 1995; Vol. *46*, pp 27−58.
(16) Frauenfelder, H.; Fenimore, P. W.; Chen, G.; McMahon, B. H. *Proc. Natl. Acad. Sci. U. S. A.* **2006**, *103*, 15469−15472.
(17) Dill, K. A. *Biochemistry* **2002**, *29*, 7133−7155.
(18) Ben-Naim, A. *Hydrophobic interactions*; Plenum Press: New York, 1980.
(19) Karplus, M.; McCammon, J. A. *Nat. Struct. Mol. Biol.* **2002**, *9*, 646−652.
(20) Privalov, P. L.; Makhatadze, G. I. *J. Mol. Biol.* **1993**, *232*, 660−679.
(21) Roux, B.; Simonson, T. *Biophys. Chem.* **1999**, *78*, 1−20.
(22) Cramer, C. J.; Truhlar, D. G. *Chem. Rev.* **1999**, *99*, 2161−2200.
(23) Baker, N. A. *Curr. Opin. Struct. Biol.* **2005**, *15*, 137−143.
(24) Honig, B.; Nicholls, A. *Science* **1995**, *268*, 1144−1149.
(25) Gilson, M. K. *Curr. Opin. Struct. Biol.* **1995**, *5*, 216−223.
(26) Scarsi, M.; Apostolakis, J.; Caflisch, A. *J. Phys. Chem. A* **1997**, *101*, 8098−8106.
(27) Feig, M.; Brooks, C. L., III. *Curr. Opin. Struct. Biol.* **2004**, *14*, 217−224.
(28) Ferrara, P.; Apostolakis, J.; Caflisch, A. *Proteins: Struct., Funct., Bioinf.* **2002**, *46*, 24−33.
(29) Knight, J. L.; Brooks, C. L. *J. Comput. Chem.* **2011**, *32*, 2909−2923.
(30) Gaillard, T.; Case, D. A. *J. Chem. Theory Comput.* **2011**, *7*, 3181−3198.
(31) Pu, M.; Garrahan, J. P.; Hirst, J. D. *Chem. Phys. Lett.* **2011**, *515*, 283−289.
(32) Juneja, A.; Numata, J.; Nilsson, L.; Knapp, E. W. *J. Chem. Theory Comput.* **2010**, *6*, 1871−1883.
(33) Alexey, O. Chapter 7 Implicit Solvent Models in Molecular Dynamics Simulations: A Brief Overview. In *Annu. Rep. Comput. Chem.*; Ralph, A. W., David, C. S., Eds.; Elsevier: New York, 2008; Vol. *Vol. 4*, pp 125−137.
(34) Feig, M.; Onufriev, A.; Lee, M. S.; Im, W.; Case, D. A.; Brooks, C. L. *J. Comput. Chem.* **2004**, *25*, 265−284.

(35) Pitera, J. W.; Swope, W. *Proc. Natl. Acad. Sci. U. S. A.* **2003**, *100*, 7587−7592.
(36) Simmerling, C.; Strockbine, B.; Roitberg, A. E. *J. Am. Chem. Soc.* **2002**, *124*, 11258−11259.
(37) Zagrovic, B.; Snow, C. D.; Shirts, M. R.; Pande, V. S. *J. Mol. Biol.* **2002**, *323*, 927−937.
(38) Hornak, V.; Okur, A.; Rizzo, R. C.; Simmerling, C. *Proc. Natl. Acad. Sci. U. S. A.* **2006**, *103*, 915−920.
(39) Wang, T.; Wade, R. C. *Proteins: Struct., Funct., Bioinf.* **2003**, *50*, 158−169.
(40) Tsui, V.; Case, D. A. *Biopolymers* **2000**, *56*, 275−291.
(41) Im, W.; Beglov, D.; Roux, B. *Comput. Phys. Commun.* **1998**, *111*, 59−75.
(42) Sharp, K. A.; Honig, B. *J. Phys. Chem.* **1990**, *94*, 7684−7692.
(43) Simonson, T. *Curr. Opin. Struct. Biol.* **2001**, *11*, 243−252.
(44) Warshel, A.; Papazyan, A. *Curr. Opin. Struct. Biol.* **1998**, *8*, 211−217.
(45) Davis, M. E.; McCammon, J. A. *Chem. Rev.* **1990**, *90*, 509−521.
(46) Lazaridis, T.; Karplus, M. *Proteins: Struct., Funct., Bioinf.* **1999**, *35*, 133−152.
(47) Masunov, A.; Lazaridis, T. *J. Am. Chem. Soc.* **2003**, *125*, 1722−1730.
(48) Wesson, L.; Eisenberg, D. *Protein Sci.* **1992**, *1*, 227−235.
(49) Hassan, S. A.; Guarnieri, F.; Mehler, E. L. *J. Phys. Chem. B* **2000**, *104*, 6478−6489.
(50) Schaefer, M.; Karplus, M. *J. Phys. Chem.* **1996**, *100*, 1578−1599.
(51) Dominy, B. N.; Brooks, C. L. *J. Phys. Chem. B* **1999**, *103*, 3765−3773.
(52) Im, W.; Lee, M. S.; Brooks, C. L. *J. Comput. Chem.* **2003**, *24*, 1691−1702.
(53) Lee, M. S.; Feig, M.; Salsbury, F. R.; Brooks, C. L. *J. Comput. Chem.* **2003**, *24*, 1348−1356.
(54) Lee, M. S.; Salsbury, J. F. R.; Brooks, C. L., III. *J. Chem. Phys.* **2002**, *116*, 10606−10614.
(55) Haberthür, U.; Caflisch, A. *J. Comput. Chem.* **2008**, *29*, 701−715.
(56) Bashford, D.; Case, D. A. *Annu. Rev. Phys. Chem.* **2000**, *51*, 129−152.
(57) Onufriev, A.; Case, D. A.; Bashford, D. *J. Comput. Chem.* **2002**, *23*, 1297−1304.
(58) Still, W. C.; Tempczyk, A.; Hawley, R. C.; Hendrickson, T. *J. Am. Chem. Soc.* **1990**, *112*, 6127−6129.
(59) Born, M. *Z. Phys.* **1920**, *1*, 45−48.
(60) Tanford, C.; Kirkwood, J. G. *J. Am. Chem. Soc.* **1957**, *79*, 5333−5339.
(61) Kirkwood, J. *J. Chem. Phys.* **1934**, *2*, 351.
(62) Baker, N. A.; Sept, D.; Joseph, S.; Holst, M. J.; McCammon, J. A. *Proc. Natl. Acad. Sci. U. S. A.* **2001**, *98*, 10037−10041.
(63) Kauzmann, W. Some Factors in the Interpretation of Protein Denaturation. In *Adv. Protein Chem.*; Anfinsen, C. B., Anson, M. L., Bailey, K., Edsall, J. T., Eds.; Academic Press: New York, 1959; Vol. *14*, pp 1−63.
(64) Tanford, C. Protein Denaturation. In *Adv. Protein Chem.*; Anfinsen, C. B., Anson, M. L., Edsall, J. T., Frederic, M. R., Eds.; Academic Press: New York, 1968; Vol. *23*, pp 121−282.
(65) Weeks, J. D.; Chandler, D.; Andersen, H. C. *J. Chem. Phys.* **1971**, *54*, 5237−5247.
(66) Wagoner, J. A.; Baker, N. A. *Proc. Natl. Acad. Sci. U. S. A.* **2006**, *103*, 8331−8336.
(67) Gallicchio, E.; Levy, R. M. *J. Comput. Chem.* **2004**, *25*, 479−499.
(68) Ooi, T.; Oobatake, M.; Némethy, G.; Scheraga, H. A. *Proc. Natl. Acad. Sci. U. S. A.* **1987**, *84*, 3086−3090.
(69) MacKerell, A. D.; Feig, M.; Brooks, C. L. *J. Am. Chem. Soc.* **2003**, *126*, 698−699.
(70) MacKerell, A. D.; Bashford, D.; Bellott; Dunbrack, R. L.; Evanseck, J. D.; Field, M. J.; Fischer, S.; Gao, J.; Guo, H.; Ha, S.; Joseph-McCarthy, D.; Kuchnir, L.; Kuczera, K.; Lau, F. T. K.; Mattos, C.; Michnick, S.; Ngo, T.; Nguyen, D. T.; Prodhom, B.; Reiher, W. E.; Roux, B.; Schlenkrich, M.; Smith, J. C.; Stote, R.; Straub, J.; Watanabe, M.; Wiórkiewicz-Kuczera, J.; Yin, D.; Karplus, M. *J. Phys. Chem. B* **1998**, *102*, 3586−3616.
(71) Neria, E.; Fischer, S.; Karplus, M. *J. Chem. Phys.* **1996**, *105*, 1902−1921.
(72) Guvench, O.; Brooks, C. L., III. *RUSH*. http://www.charmm.org/documentation/c36b1/rush.html (accessed 11/30/2012).
(73) Sharp, K. A.; Nicholls, A.; Friedman, R.; Honig, B. *Biochemistry* **1991**, *30*, 9686−9697.
(74) Coles, M.; Bicknell, W.; Watson, A. A.; Fairlie, D. P.; Craik, D. J. *Biochemistry* **1998**, *37*, 11064−11077.
(75) Jarvet, J.; Danielsson, J.; Damberg, P.; Oleszczuk, M.; Gräslund, A. *J. Biomol. NMR* **2007**, *39*, 63−72.
(76) Crescenzi, O.; Tomaselli, S.; Guerrini, R.; Salvadori, S.; D'Ursi, A. M.; Temussi, P. A.; Picone, D. *Eur. J. Biochem.* **2002**, *269*, 5642−5648.
(77) *Insight II*, version 2000; Accelrys Inc.: San Diego, CA, 2000.
(78) Loncharich, R. J.; Brooks, B. R.; Pastor, R. W. *Biopolymers* **1992**, *32*, 523−535.
(79) Brooks, B. R.; Bruccoleri, R. E.; Olafson, B. D.; States, D. J.; Swaminathan, S.; Karplus, M. *J. Comput. Chem.* **1983**, *4*, 187−217.
(80) Brooks, B. R.; Brooks, C. L.; Mackerell, A. D.; Nilsson, L.; Petrella, R. J.; Roux, B.; Won, Y.; Archontis, G.; Bartels, C.; Boresch, S.; Caflisch, A.; Caves, L.; Cui, Q.; Dinner, A. R.; Feig, M.; Fischer, S.; Gao, J.; Hodoscek, M.; Im, W.; Kuczera, K.; Lazaridis, T.; Ma, J.; Ovchinnikov, V.; Paci, E.; Pastor, R. W.; Post, C. B.; Pu, J. Z.; Schaefer, M.; Tidor, B.; Venable, R. M.; Woodcock, H. L.; Wu, X.; Yang, W.; York, D. M.; Karplus, M. *J. Comput. Chem.* **2009**, *30*, 1545−1614.
(81) Ryckaert, J.; Ciccotti, G.; Berendsen, H. *J. Comput. Phys.* **1977**, *23*, 327−341.
(82) Kabsch, W.; Sander, C. *Biopolymers* **1983**, *22*, 2577−2637.
(83) De Loof, H.; Nilsson, L.; Rigler, R. *J. Am. Chem. Soc.* **1992**, *114*, 4028−4035.
(84) Hovmoller, S.; Zhou, T.; Ohlson, T. *Acta Crystallogr., Sect. D* **2002**, *58*, 768−776.
(85) Levitt, M. *J. Mol. Biol.* **1983**, *168*, 621−657.
(86) Sammon, J. W., Jr. *IEEE Trans. Comput.* **1969**, *C-18*, 401−409.
(87) Nina, M.; Beglov, D.; Roux, B. *J. Phys. Chem. B* **1997**, *101*, 5239−5248.